Chinese Chemical Letters 33 (2022) 428–433

Contents lists available at ScienceDirect

Chinese Chemical Letters

journal homepage: www.elsevier.com/locate/cclet

The role of $NiFe_2O_4$ nanoparticle in the anaerobic digestion (AD) of waste activated sludge (WAS)

Lihong Zhou[a], Xueqian Yan[b], Xiangjun Pei[a,c], Jie Du[d], Rui Ma[b], Jin Qian[b,*]

[a] College of Ecology and Environment, Chengdu University of Technology, Chengdu 610000, China
[b] School of Chemistry and Chemical Engineering, Northwestern Polytechnical University, Xi'an 710072, China
[c] State Key Laboratory of Geohazard Prevention and Geoenvironment Protection, Chengdu University of Technology, Chengdu 610000, China
[d] Jiuzhaigou Administration Bureau, Aba 623402, China

ARTICLE INFO

Article history:
Received 4 April 2021
Revised 28 April 2021
Accepted 21 June 2021
Available online 3 July 2021

Keywords:
Anaerobic digestion (AD)
Waste activated sludge (WAS)
Methane production
$NiFe_2O_4$
Direct interspecies electron transfer (DIET)
Microbial community analysis

ABSTRACT

Anaerobic digestion (AD) is a promising technology for the treatment of waste activated sludge (WAS) with energy recovery. However, the low methane yield and slow methanogenesis limit its broad application. In this study, the $NiFe_2O_4$ nanoparticles (NPs) were fabricated and applied as a conductive material to enhance the AD *via* promoting the direct interspecies electron transfer (DIET). The crystal structure, specific surface area, morphology and elemental composition of the as-prepared $NiFe_2O_4$ NPs were characterized by X-ray diffraction (XRD), Brunauer-Emmett-Teller (BET), scanning electron microscopy (SEM) and energy dispersive spectroscopy (EDS). The biochemical methane potential (BMP) test was performed (lasting for 35 days) to evaluate the energy recovery in AD with the addition of the $NiFe_2O_4$ NPs. The results illustrate that $NiFe_2O_4$ NPs could accelerate both the hydrolysis, acidogenesis and methanogenesis, *i.e.*, the cumulative methane production and daily methane yield increased from 96.76 ± 1.70 mL/gVS and 8.24 ± 1.26 mL gVS^{-1} d^{-1} in the absence of $NiFe_2O_4$ NPs (Group A) to 123.69 ± 3.20 mL/gVS and 9.71 ± 0.77 mL gVS^{-1} d^{-1} in the presence of $NiFe_2O_4$ NPs (Group B). The model simulation results showed that both the first-order kinetic model and the modified Gompertz model can well simulate the experimental results. The hydrolysis rate constant k increased from 0.04 ± 0.01 d^{-1} in Group A to 0.06 ± 0.01 d^{-1} in Group B. And the maximum methane production potential and activity were both improved after adding $NiFe_2O_4$. The microbial community analysis revealed that the microorganisms associated with hydrolysis and acidogenesis were more abundant in the presence of $NiFe_2O_4$. And the methanogenic archaea were enriched to a larger extent, resulted in the higher methanogenesis activities *via* dosing $NiFe_2O_4$.

The waste activated sludge (WAS) is generated as an inevitable byproduct in the wastewater treatment plants (WWTPs) [1]. Without proper treatment, the WAS will cause the secondary pollution to the ecological system as well as impose the detrimental effects on human health [2–6]. In China, as much as 60 million tons of WAS is produced in 2020, and the cost for traditional sludge treatment and disposal accounts for 25%–65% of total operating costs in WWTPs [7]. Therefore, the critical issue of WAS produced every year drives us to provide a more promising solution for the sustainable sludge disposal and treatment.

Currently, the WAS treatment is generally dependent on landfilling, incineration, aerobic compost, synthesis of sludge-based functional materials, aerobic digestion and anaerobic digestion [8–10]. Among them, anaerobic digestion (AD) is preferred to other technologies in the current society, in view of the resource (in the form of volatile fatty acids, *etc.*) and energy (in the from of methane) recovery achievable in the side-stream treatment of WWPTs. With the aid of AD, in the main-stream the sewage can be economically and sustainable treated in a energy-neutral (ultimate AD product of methane for electricity generation) system [11]. However, the broad application AD is always hindered by the unsatisfactory methane gas yield due to the slow hydrolysis rate of large organic particles in WAS. To address this situation, the pretreatment (*e.g.*, mechanical, chemical, thermal and biological) were frequently implemented prior to AD to improve the hydrolysis performances and enhance the methane production in previous studies [12–15]. But the large amounts of energy and chemicals are consumed in these approaches [16].

Establishing direct interspecies electron transfer (DIET)-based syntrophic metabolism with conductive materials has been considered as a promising strategy to achieve effective methano-

* Corresponding author.
E-mail addresses: qianjin@nwpu.edu.cn, qianjin131@yahoo.com.hk (J. Qian).

https://doi.org/10.1016/j.cclet.2021.06.055
1001-8417/

genesis and stable AD process [17]. Until now, many conductive materials have been confirmed to be able to improve the performance of methanogenesis. For example, Fe(III) oxides such as Fe_3O_4 particles could serve as electron conduits to stimulate direct interspecies electron transfer (DIET) from propionate-oxidizing acetogens to carbon dioxide-reducing methanogens to produce methane [18]. Graphite rod have been reported to accelerate the syntrophic conversion of alcohols and volatile fatty acids (VFAs) to methane through DIET in defined co-cultures of *G. metallireducens* and *Methanosarcina* barkeri along with enriched population of *Methanosaeta* and *Methanosarcina* sp. attaching to the conductive materials [19]. Nickel ferrite ($NiFe_2O_4$), a ferrite exhibiting the typical spinel structure, good chemical and thermal stability, as well as superior magnetic and conductive properties [20,21], has been practiced to enhance the methane gas generation in the AD of wastewater. However, its application for AD of the WAS was unavailable so far. And the role of $NiFe_2O_4$ in energy recovery (as methane gas) from the WAS deserved to be explored and discussed in detail.

In the present study, we aim to fabricate the $NiFe_2O_4$ nanoparticle (NP) *via* the hydrothermal method. The physiochemical properties of the as-prepared NP were thoroughly characterized herein. Moreover, the role of $NiFe_2O_4$ NP in AD of the WAS was explored *via* the biochemical methane potential (BMP) test in the batch mode. To further reveal the potential mechanism of the enhanced BMP derived from $NiFe_2O_4$ NP, the microbial community was analyzed by high-throughput 16S rRNA pyrosequencing.

The WAS and inoculum used in this study were collected from the secondary sedimentation tank and sludge thickening tank, respectively in a municipal WWPT located in the Xi'an, China. The raw sludge was concentrated through gravitationally settled for 12 h before they are stored at 4 °C. The main physicochemical characteristics of both WAS and inoculum are shown in Table S1 (Supporting information).

Nickel(II) chloride hexahydrate ($NiCl_2{\cdot}6H_2O$), iron(III) nitrate nonahydrate ($Fe(NO_3)_3{\cdot}9H_2O$), sodium hydroxide were purchased from Shanghai McLin Biochemical Technology Co., The Milliq-Q water (18.25 MΩ/cm) was used to prepare all the solutions throughout this study.

2.0 g of ferric nitrate ($Fe(NO_3)_3{\cdot}9H_2O$) and 0.96 g of nickel nitrate($NiCl_2{\cdot}6H_2O$) were simultaneously dissolved in 30 mL of deionized water by magnetic stirring, thus the molar ratio of Fe^{3+} to Ni^{2+} was 1.5:1. The pH was adjusted to 13.0 by adding 6 mol/L NaOH under vigorous stirring. The mixed solution was then transferred into a 50 mL Teflon lined autoclave. And the tightly-sealed autoclave was heated at 210 °C for 20 h in a muffle furnace. Afterward, the material sample was carefully washed for three times with ultrapure water and ethanol, followed by drying at 80 °C in an oven until completely dewatering.

X-ray diffraction (XRD) patterns of the fabricated materials were examined via an X-ray diffraction instrument (Shimadzu 7000) equipped with Cu-kα radiation (λ = 1.54 Å) within the 2θ range of 20° to 80° at a scanning rate of 8°/min [22]. Textural properties including specific surface area and pore size distribution of the nanocomposites were determined using the Brunauer-Emmett-Teller (BET) and Barett-Joyner-Halenda (BJH) methods. The calculations were based on N_2 adsorption-desorption at 77 K using a specific surface area analyzer (Beishide 3H-2000PS2, China). The morphology and element composition were examined using scanning electron microscopy (SEM, TESCAN VEGA 3 LMH) equipped with the energy dispersive spectroscopy (EDS).

In this study, BMP tests were performed on an Automatic Methane Potential Test System II (Bioprocess Control, Sweden) in which a series of serum bottles (working volume: 400 mL) equipped with plastic caps including agitators and rubber stoppers were employed as the batch digesters. All BMP tests were conducted in triplicates. Each bath reactor consisted of 272.14 mL inoculum and 127.86 mL WAS (the mass ratio of substrate (WAS) to inoculum was 0.5), with 0 and 0.25 g/L $NiFe_2O_4$ NPs dosed in the Group A and B, respectively. In order to determine the biogas productivity from the endogenous respiration of the inoculum, the blank control group with 127.86 mL WAS and 272.14 mL H_2O added was also developed. Once the reactors were loaded, the analytic-graded nitrogen gas was purged into each digester to eliminate the headspace oxygen at a flow rate of 1 L/min for 1 min. After being sealed, all the reactors were placed in a water bath controlled at 35 ± 1 °C. The daily and cumulative biomethane productions in BMP test were recorded using an in-built data-logger in the AMPTS II. The entire digestion lasted for 35 days. And the BMP test was stopped when methane production fell to insignificant levels.

The pH was determined using a pH-meter (pHs-3C, Leici Co., Ltd., Shanghai). The protein contents were quantified by the modified Lowry method [23], and Anthrone-sulfuric acid method was adopted to measure polysaccharides [24]. The measurements for soluble chemical oxygen demand (SCOD), total solids (TS) and volatile solids (VS) were undertaken according to the standard methods [25].

The batch tests results regarding the impact of $NiFe_2O_4$ NPs on the methanogenic process were simulated by both first-order reaction kinetic model and the modified Gompertz equation (Eqs. 1 and 2) using Origin 8.5 software (Origin Cop., USA).

$$M(t) = M_0 \times (1 - \exp(-kt)) \tag{1}$$

$$M(t) = M_0 \times \exp\left\{-\exp\left[\frac{R_{\max} \times e}{M_0}(\lambda - t) + 1\right]\right\} \tag{2}$$

where *M(t)* is the cumulative methane over time (mL/gVS), M_0 is the final methane yield (mL/gVS), *k* is the hydrolysis rate constant (d^{-1}), R_{max} is the maximum methane production rate (mL gVS^{-1} d^{-1}), λ is the lag phase (days), *t* is the duration of the incubation period (days) and *e* is Euler's number (2.71828).

The microbial communities of digested sludge with and without $NiFe_2O_4$ NPs dosing after BMP tests were analyzed *via* the high-throughput 16S rRNA gene sequencing. Sludge samples were sent to Majorbio Bio-Pharm Technology Co., Ltd. (Shanghai, China) for DNA extraction and PCR amplification. The E.Z.N.A soil Kit (Omega Bio-Tek, Norcross, GA, U.S.) was used for the microbial DNA extraction in sludge samples. The NanoDrop 2000 UV–vis spectrophotometer (Thermo Scientific, Wilmington, USA) was used for measuring the final DNA concentration and purification, while the DNA quality was checked by 1% agarose gel electrophoresis. The PCR amplification were performed using a thermocycler PCR system (GeneAmp9700, ABI, USA) with primers 515FmodF (5′-GTGYCAGCMGCCGCGGTAA-3′) and 806RmodR (5′-GGACTACNVGGGTWTCTAAT-3′). The PCRs have executed in triplicate 20 μL reaction mixtures, containing 4 μL of 5 × FastPfu Buffer, 2 μL of 2.5 mmol/L dNTPs, 0.8 μL of each primer (5 μmol/L), 0.4 μL of FastPfu Polymerase, 0.2 μL of BSA and 10 ng of template DNA. The AxyPrep DNA Gel Extraction Kit (Axygen Biosciences, Union City, CA, USA) was used together with quantification using the QuantiFluor-ST system (Promega, USA) for the first extraction of PCR products from a 2% agarose gel and for further purification [26]. And then the PCR amplification results were divided at the Operational Classification Unit (OTU) level.

The crystal structure of the as-prepared sample was analyzed with XRD and the results are shown in Fig. 1a. All the diffraction peaks of $NiFe_2O_4$ at the 2θ values of 18.60°, 30.48°, 35.86°, 43.58°, 53.80°, 57.62°, 63.20°, 71.58° and 74.66° are indexed to (111), (220), (311), (400), (422), (511), (440), (620) and (533) crystal planes of spinel $NiFe_2O_4$ (JCPDS No. 10–0325), respectively [27]. Thus, the

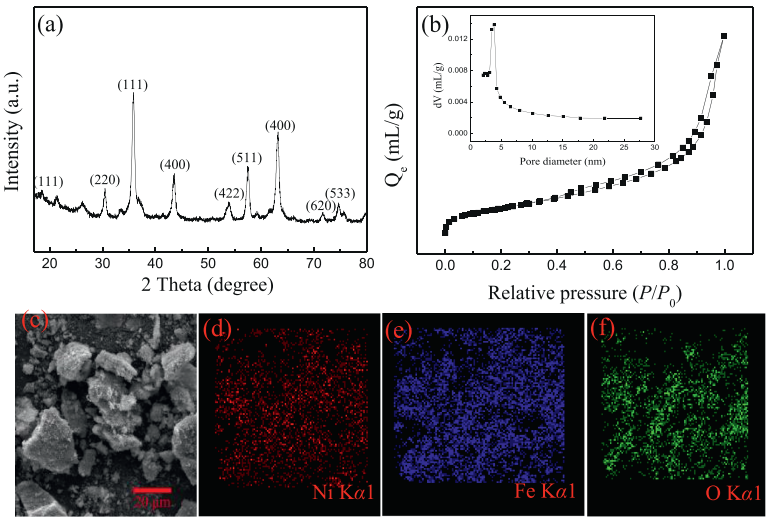

Fig. 1. (a) XRD pattern of $NiFe_2O_4$, (b) Nitrogen adsorption/desorption isotherm and the corresponding pore size distribution curve of $NiFe_2O_4$, (c) SEM image of $NiFe_2O_4$ and (d-f) EDS elemental mapping of $NiFe_2O_4$.

XRD results demonstrate the high crystallinity of the as-prepared material, and no other impurity phases were detected.

Textural properties of $NiFe_2O_4$ NPs were characterized by nitrogen adsorption-desorption test and the result is displayed in Fig. 1b. As it can be seen from the adsorption-desorption graph, the sample exhibits typical IV isotherms, indicating the mesoporous structure of the material. The specific surface area and pore properties of the material were calculated by BET and BJH models. As shown in Table S2 (Supporting information), the specific surface area of the $NiFe_2O_4$ NPs is as high as 41.58 m^2/g. The large specific surface area is beneficial for the contact of nanoparticles with microorganisms and AD substrate, thus promoting the AD process [28].

The SEM image of $NiFe_2O_4$ is presented in Fig. 1c and it indicates that the $NiFe_2O_4$ exhibits an irregular shaped plate-like nanostructure with non–uniform grain sizes. The EDS results confirm the presence of Ni, Fe and O elements in the NP, as illustrated in Figs. 1d–f.

The pH is an essential metric to evaluate the stability of AD reactors, as it is associated with metabolic products such as VFAs, ammonia and organic acids [7]. As shown in Fig. 2a, the pH in the non-$NiFe_2O_4$ reactor (Group A) fluctuated in the range of 6.81–7.52. In contrast, the reactor with $NiFe_2O_4$ NPs (Group B) was more stable, which remained between 6.81 and 7.29.

The tendency of SCOD, protein and polysaccharide changes during AD could describe the solubilization of organic fractions in WAS and the subsequent utilization by the acidogens and methanogens [29]. Figs. 2b–d show the variation of organic matters in both groups throughout the anaerobic process (35 days). As expected, SCOD in anaerobic digestion constantly increased during the initial 15 days, due to the endogenous biomass decay (releasing the soluble organic matters from the organisms) and slow methanogenesis (see the results below in the methanogenic analysis) [30]. On day 15, the SCOD levels of Group B and Group A peaked at 2956.85 ± 2.37 mg/L and 2735.46 ± 4.70 mg/L, respectively. The results suggested that the presence of $NiFe_2O_4$ in AD could promote sludge solubilization. Afterwards, a declined trend was observed in both AD systems due to the balance established gradually between the acidification process and methanogenesis process [31]. And finally the SCOD dropped to 1378.92 ± 2.05 mg/L and 1658.26 ± 2.54 mg/L, respectively. The changing trends of protein and polysaccharide in AD systems were consistent with that of SCOD, which reached the maximum level on day 15 before gradually decreased. It is obvious that the decomposition rate of protein and polysaccharide in Group B was rapid than that in Group A, indicating that $NiFe_2O_4$ NPs can also enhance the acetogenesis. This may be due to the enrichment of protein and polysaccharide-consuming bacteria with the addition of $NiFe_2O_4$ NPs, as illustrated in microbial sequencing analysis. All the above results confirmed that the addition of $NiFe_2O_4$ NPs could accelerate both the decomposition of sludge and consumption of biodegradable organic matters, thus contributing to high methane production in Group B (see the results are shown in the methanogenic analysis below).

The removal of VS and TS in both digesters were compared, as shown in Table S3 (Supporting information). When the $NiFe_2O_4$ (0.25 g/L) was introduced to the AD process, the VS and TS removal efficiencies reached 22.42% and 25.11%, respectively. The results in the Group A were lower than those in the Group B, with the VS and TS removal efficiencies of 14.75% and 16.49%, respectively. The higher TS/VS removal in Group B could be mainly ascribed to the enhanced hydrolysis and degradation of protein, polysaccharide-like organic matters during the digestion process in the presence of $NiFe_2O_4$ NPs (see the results are shown in the organic degradation analysis).

Both the cumulative methane generation and daily methane yield are displayed in Figs. 2e and f. With the addition of $NiFe_2O_4$ NPs, the maximum methane yield was enhanced by 27.83%, *i.e.*, increased from 96.76 ± 1.70 mL/gVS to 123.69 ± 3.20 mL/gVS (Fig. 2e), supporting the positive impact of the $NiFe_2O_4$ in methane production in AD. This finding can be explained by two reasons. First, $NiFe_2O_4$ NPs serve as conduits for electron transfer in the AD system, hence stimulating the direct interspecies electron transfer (DIET) between the bacterial and archaeal communities. Second, Fe and Ni ions contained in the $NiFe_2O_4$ NPs are known as the essential micronutrients for enzyme immobilization as well as supporting metabolisms during AD process, so as to enrich the functional miroorganisms and activities of key enzymes/co-enzymes [31].

Fig. 2f informs that daily biogas yield in two digesters were within the range of 0–8.24 mL gVS^{-1} d^{-1} (Group A) and 0–9.71 mL gVS^{-1} d^{-1} (Group B). As seen in Fig. 2f, the methanogenesis (indicated by the methane gas generation) was initiated immediately on the first day of AD in both groups. And there were three key peaks for the profile of methane yield *versus* time in both systems. The first peak of methane yield appearing on Days 6 to 7

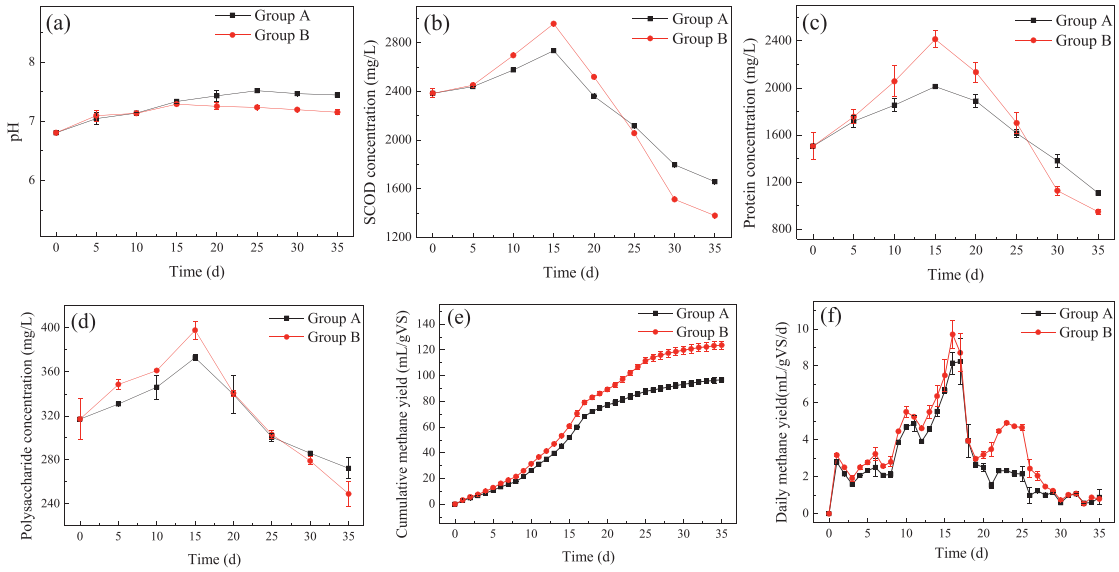

Fig. 2. Profile of (a) pH; (b) SCOD concentration; (c) protein concentration; (d) polysaccharide concentration; (e) the cumulative methane yield; (f) the daily methane yield *versus* time (d) in both AD systems. The error bar represents the standard deviation of three repeated experiments.

may correspond to the initial transformation of the available soluble organic substrates in WAS. The second peak on Day 10 could be related to easily degraded compounds generated in the early stage of the reaction, and the third peak on Days 15–18 may be attributed to the slow conversion of non-readily biodegradable compounds to methane gas [32]. Thereafter, methane production in all reactors gradually ceased.

To further understand the effect of $NiFe_2O_4$ NPs on AD (especially on the methane production), first-order reaction kinetic model and the modified Gompertz model were adopted to simulate these experimental results. Tables S4 and S5 (Supporting information) show the key analysis results including k, M_0, R_{max} and λ. As the correlation coefficients (R^2) were all $>$ 0.95, the two models well captured the experimental data. After adding $NiFe_2O_4$ NPs, the hydrolysis rate constant increased to 0.06 $\pm$ 0.01 d^{-1}, which was 1.5 folds of that in Group A (0.04 $\pm$ 0.01 d^{-1}). Thus in addition to the SCOD results shown in Fig. 2b, the modeling simulation further confirms the enhanced hydrolysis of WAS in the presence of $NiFe_2O_4$. The maximum methane production rate (R_{max}) can be used to evaluate the methanogenic activities in AD reactor [33]. As shown in Table S5, R_{max} elevated from 5.37 $\pm$ 0.12 mL gVS^{-1} d^{-1} (Group A) to 6.20 $\pm$ 0.25 mL gVS^{-1} d^{-1} (Group B). Similarly, the M_0 value of the Group B with $NiFe_2O_4$ NPs addition was higher than that of the Group A, demonstrating the $NiFe_2O_4$ NPs did have positive impacts on methane production. The lag phase (λ) indicated the period required for the microorganisms in the anaerobic system to acclimate to the new environment [34]. Comparatively, the calculated λ was shorter in Group B, likely due to the fact that the nanomaterials containing micronutrients can promote the synthesis of enzymes and cell components required for microbial growth [35].

The microbial diversity and distribution in both Groups A and B were revealed at phylum, class, family and genus levels *via* the high-throughput 16S rRNA analysis, to further understand the mechanism of the enhanced AD in the presence of $NiFe_2O_4$ NPs. As shown in Fig. 3a, at the phylum level, *Chloroflexi, Proteobacteria* and *Bacteroidetes* were dominant in both digesters and accounted for 59% to 63% of the total bacterial community, which are also found to be the dominant phyla of AD process as previously reported [36]. Compared with the Group A, these three phyla were enriched to a larger degree in Group B. *Proteobacteria* is a group of anaerobic, mesophilic and protein-utilizing microorganisms [37]. It could convert proteins-like organic matters into short-chain fatty acids as the available substrate for the subsequent methanogenesis [38]. The members affiliated to *Bacteroidetes* played a crucial role in hydrolyzing polysaccharides under anaerobic conditions [39]. Thus the $NiFe_2O_4$ NPs may enhance the AD performance *via* accelerating the degradation of protein and polysaccharide in WAS. In addition, *Chloroflexi* can produce hydrolytic enzymes for the degradation of soluble microbial products including soluble protein and soluble polysaccharide *etc* [40].

As illustrated in Fig. 3b, *Bacteroidia, Gammaproteobacteria* and *Anaerolineae* were identified as the predominant bacteria at the class level in two groups. The relative abundance of *Anaerolineae* in Group B was higher than that in group A. *Anaerolineae* belongs to phylum of *Chloroflexi*, which is mainly responsible for the bio-conversion of complex organic macromolecules to organic acids [41]. *Gammaproteobacteria*, under the phylum of *Proteobacteria* could decompose glucose and long-chain fatty acids [42]. These results demonstrated that the AD systems with the $NiFe_2O_4$ NPs can accelerate the hydrolysis of refractory macromolecular substrates to short chain acids, H_2 and other intermediates, leading to accelerating the methanogenesis [43]. It is also noteworthy that, *Alphaproteobacteria, Bacteroidia*, and *Synergistia* could act as electron-donor bacteria during the DIET and play the siginificant roles in the acetogenesis [44]. The higher abundances of *Alphaproteobacteria, Bacteroidia* and *Synergisita* in Group B than that of the Group A suggested that the $NiFe_2O_4$ NPs can promote the growth of electron-donor bacteria. *Methanomicrobia* and *Methanobacteria* were the well-known and most abundant methanogenic archaea at the class levels [45] in both groups (Fig. 3b). The *Methanomicrobia* can act as electron-acceptor archaea for reducing CO_2 into methane [46]. And the more enriched *Methanomicrobia* in Group B with $NiFe_2O_4$ NPs resulted in the high methanogenic activity as shown in the methanogenic analysis

At the family level (Fig. 3c), the relative abundance of *Synergistaceae* and *Syntrophaceae* increased by 26.00% and 16.22% with the addition of $NiFe_2O_4$ NPs, respectively. These two microbes are mainly responsible for the acetogenesis in the established DIET system [47]. Community heatmap analysis at the genus level is shown in Fig. 3d. The total relative abundance of *norank_Caldilineaceae*, which belong to phylum *Chloroflexi* and could

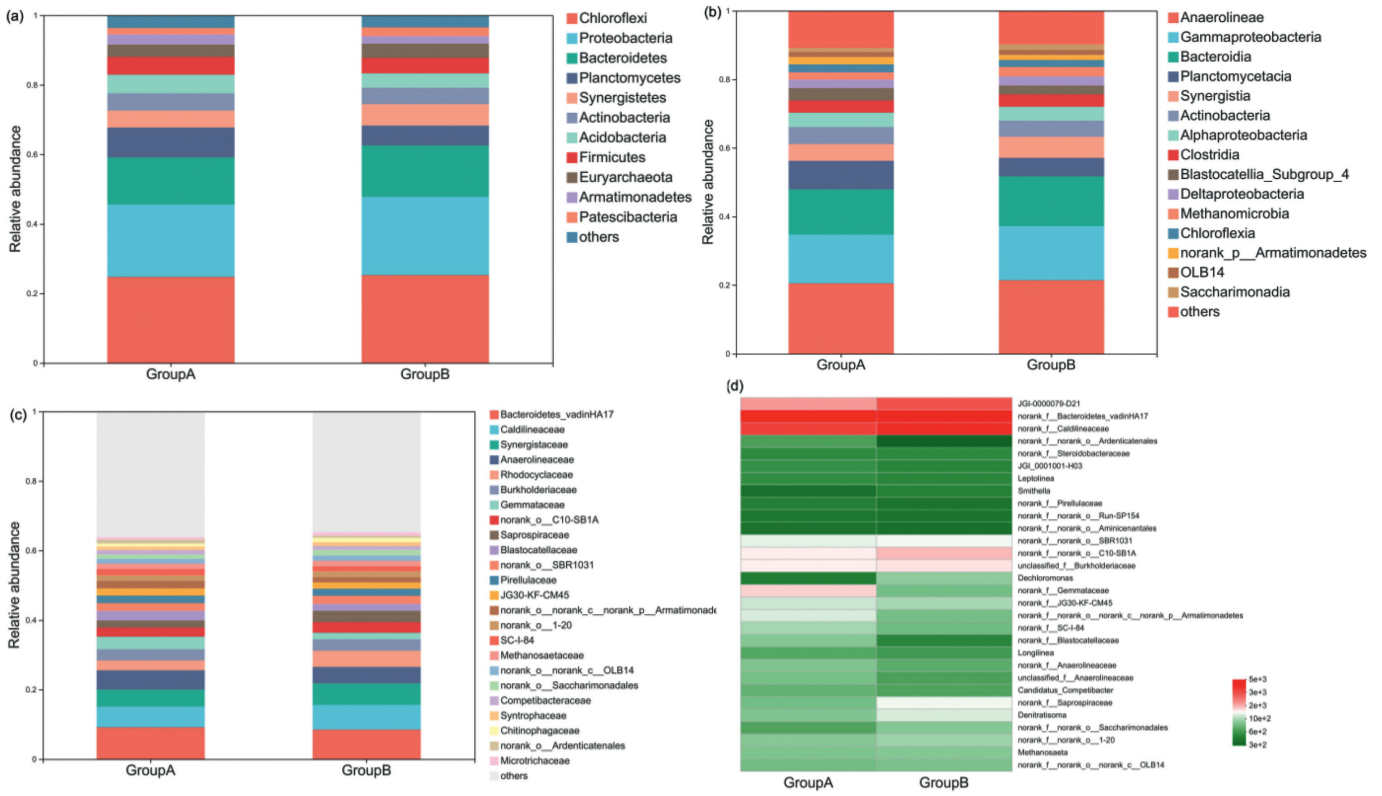

Fig. 3. Community structure at (a) phylum, (b) class and (c) family levels of microorganisms in Groups A and B. (d) Community heatmap on genus level of microorganisms in Groups A and B.

utilize sucrose, glucose and *N*-acetyl-glucosamine-like organic matters [48], were 19.84% higher in Group B compared with Group A. *norank_Bacteroidetes_vadinHA17* was responsible for hydrolysis and fermentation of various pollutants in AD system [49], the level of which was also higher in Group B (9.13%) than Group A (8.47%).

The role of $NiFe_2O_4$ NPs in AD of WAS was firstly examined in this study. The cumulative methane production and daily average methane yield in the presence of $NiFe_2O_4$ NPs were enhanced by 27.83% and 17.84% respectively, and the VS removal rate was increased by 7.67%. The model simulation results showed that the addition of $NiFe_2O_4$ nanoparticles significantly improves the hydrolysis rate and shortens the lag phase. The microbial community analysis revealed that the levels of *Chloroflexi, Proteobacteria* and *Bacteroidetes* were elevated after dosing $NiFe_2O_4$, thereby improving the hydrolysis performance and providing more substrates for subsequent methane production. In addition, the higher abundance of electron-donor microorganisms (*Acetobacter*, such as *Bacteroides* and *Synergist*) and electron-acceptor microorganisms (methanogens, such as *methanogens*) in the presence of $NiFe_2O_4$ NP, resulted in the enhanced methane production *via* promoting the DIET.

Declaration of competing interest

The authors declare that they have no known competing financial interests or personal relationships that could have appeared to influence the work reported in this paper.

Acknowledgments

This work was financially supported by the Fundamental Research Funds for Central Universities (Nos. 3102019AX18 and 310201911cx021), and the Specialized Fund for the Post-Disaster Reconstruction and Heritage Project ion in Sichuan Province (No. 5132202019000128).

Supplementary materials

Supplementary material associated with this article can be found, in the online version, at doi:10.1016/j.cclet.2021.06.055.

References

[1] H. Chen, M. Tang, X. Yang, et al., Chem. Eng. J. 408 (2021) 127251.
[2] J. Peng, Y. He, C. Zhou, et al., Chin. Chem. Lett. 32 (2021) 1626–1636.
[3] Q. Wu, H. Li, X. Hu, et al., Chin. Chem. Lett. 31 (2020) 2825–2830.
[4] L. Wei, X. Xia, F. Zhu, et al., Water Res. 181 (2020) 115903.
[5] Y. Li, Y. Fu, M. Zhu, Appl. Catal. B 260 (2020) 118149.
[6] S. Lan, Y. Chen, L. Zeng, et al., J. Hazard. Mater. 393 (2020) 122448.
[7] M. Zhang, Y. Wang, Bioresour. Technol. 313 (2020) 123695.
[8] H. Zhang, S. Song, L. Sun, et al., Chin. Chem. Lett. 31 (2020) 1432–1437.
[9] L. Wei, F. Zhu, Q. Li, et al., Environ. Int. 144 (2020) 106093.
[10] H. Wang, W. Guo, B. Liu, et al., Appl. Catal. B 279 (2020) 119361.
[11] A.M. Abdelrahman, H. Ozgun, R.K. Dereli, et al., Crit. Rev. Environ. Sci. Technol. 51 (2021) 2119–2157.
[12] P. Neumann, S. Pesante, M. Venegas, G. Vidal, Rev. Environ. Sci. Biotechnol. 15 (2016) 173–211.
[13] W. Mussoline, G. Esposito, A. Giordano, P. Lens, Crit. Rev. Environ. Sci. Technol. 43 (2013) 895–915.
[14] G. Zhen, X. Lu, H. Kato, et al., Renew. Sustain. Energy Rev. 69 (2017) 559–577.
[15] J. Ariunbaatar, A. Panico, G. Esposito, et al., Appl. Energy 123 (2014) 143–156.
[16] W. Wei, Z. Cai, J. Fu, et al., Chem. Eng. J. 351 (2018) 1159–1165.
[17] Z. Zhao, Y. Li, X. Quan, Y. Zhang, Water Res. 115 (2017) 266–277.
[18] C.C. Viggi, S. Rossetti, S. Fazi, et al., Environ. Sci. Technol. 48 (2014) 7536–7543.
[19] P. Gahlot, B. Ahmed, S.B. Tiwari, et al., Environ. Technol. Innov. 20 (2020) 101056.
[20] Z. Wei, H. Li, J. Wu, et al., Chin. Chem. Lett. 31 (2020) 177–180.
[21] J. Liu, J. Shen, M. Li, L. Guo, Chin. Chem. Lett. 26 (2015) 1478–1484.
[22] R. Yin, Y. Chen, S. He, et al., J. Hazard. Mater. 388 (2020) 121996.
[23] J. Zhao, G. Hu, Y. Huang, et al., Chin. Chem. Lett. 32 (2020) 1331–1340.
[24] Q. Xu, X. Liu, Y. Fu, et al., Bioresour. Technol. 267 (2018) 141–148.
[25] T. Luo, H. Huang, Z. Mei, et al., Chin. Chem. Lett. 30 (2019) 1219–1223.
[26] Y. Luo, J. Yao, X. Wang, et al., Sci. Total Environ. 703 (2020) 135031.
[27] J. Qu, T. Che, L. Shi, et al., Chin. Chem. Lett. 30 (2019) 1198–1203.

[28] Y. Qin, X. Yin, X. Xu, et al., Bioresour. Technol. 303 (2020) 122919.
[29] B. Wu, Q. Yang, F. Yao, et al., Bioresour. Technol. 294 (2019) 122235.
[30] B. Yu, D. Zhang, X. Dai, et al., RSC Adv. 6 (2016) 21090–21098.
[31] X. Zhu, E. Blanco, M. Bhatti, A. Borrion, Sci. Total Environ. 757 (2021) 143747.
[32] J. Li, M. Zhang, Z. Ye, C. Yang, J. Environ. Sci. 76 (2019) 267–277.
[33] Y. Zhang, Z. Yang, R. Xu, et al., Sci. Total Environ. 683 (2019) 124–133.
[34] W. Zhang, Q. Wei, S. Wu, et al., Appl. Energy 128 (2014) 175–183.
[35] Y. Chen, Z. Yang, Y. Zhang, et al., Bioresour. Technol. 304 (2020) 123016.
[36] L. Wei, X. An, S. Wang, et al., Bioresour. Technol. 244 (2017) 261–269.
[37] H.J. Kang, S.H. Lee, T.G. Lim, et al., Bioresour. Technol. 322 (2021) 124587.
[38] E.T. Papoutsakis, Curr. Opin. Biotechnol. 19 (2008) 420–429.
[39] H. Hou, L. Duan, B. Zhou, et al., Chin. Chem. Lett. 31 (2020) 543–546.
[40] C. Cheng, Z. Zhou, Z. Qiu, et al., Bioresour. Technol. 249 (2018) 298–306.
[41] Z. He, C. Yang, C. Tang, et al., Bioresour. Technol. 322 (2021) 124536.
[42] C. Wang, Y. Liu, S. Jin, et al., Bioresour. Technol. 272 (2019) 162–170.
[43] G. Chen, W. Wu, J. Xu, Z. Wang, Bioresour. Technol. 329 (2021) 124864.
[44] X. Liu, L. Shi, J. Gu, Biotechnol. Adv. 36 (2018) 1815–1827.
[45] Z. Wang, S. Yun, J. Shi, et al., Bioresour. Technol. 311 (2020) 123519.
[46] J.H. Park, H.J. Kang, K.H. Park, H.D. Park, Bioresour. Technol. 254 (2018) 300–311.
[47] L. Yang, B. Si, Y. Zhang, et al., J. Clean. Prod. 276 (2020) 122836.
[48] D. Ruan, Z. Zhou, H. Pang, et al., Bioresour. Technol. 289 (2019) 121643.
[49] C. Chen, W.S. Guo, H.H. Ngo, et al., Renew. Energy 111 (2017) 620–627.